

1 **Back-arc underplating provided crustal accretion affecting topographic and** 2 **sedimentation in the Adria microplate**

3 Paolo Mancinelli^{1*}, Vittorio Scisciani¹, Cristina Pauselli², Gérard M. Stampfli³, Fabio Speranza⁴, Ivana
4 Vasiljevic⁵

5 * Corresponding author: paolo.mancinelli@unich.it ORCID: 0000-0003-4524-3199

6 ¹ Dipartimento di Ingegneria e Geologia, Università G. D'Annunzio di Chieti-Pescara.

7 ² Dipartimento di Fisica e Geologia, Università degli Studi di Perugia

8 ³ Institute of Earth Sciences, Université de Lausanne

9 ⁴ Istituto Nazionale di Geofisica e Vulcanologia

10 ⁵ Faculty of Mining and Geology, University of Belgrade

11

12 **Magmatic underplating in crustal formation and evolution is often related to plate tectonics and**
13 **dynamics. Despite underplating is very common in extensional settings where it is associated to crustal**
14 **breakup, this process is also responsible of large-scale flood basalt volcanic districts. Conversely, in**
15 **compressional settings the role of underplated volumes is less obvious and the effects on crustal**
16 **accretion in the back-arc area are still questioned. Traditionally, the distinctive features of magmatic**
17 **underplating are high P- and S-wave velocity, high density and high Vp/Vs of the intruded volume when**
18 **compared to surrounding crust. More in general, the products and crustal structures derived from**
19 **underplating processes may range in a wide spectra, mostly depending on the geodynamic setting.**
20 **Supported by evidences of deep crustal sources for the observed magnetic anomalies in Central Italy and**
21 **by outcropping gabbros in the Croatian archipelago, we model the observed gravity and magnetic**
22 **anomalies in the Central Adriatic Sea and surroundings. We find that the major magnetic anomalies in**
23 **the area are related to wide underplated Permian gabbros and propose that the underplated volumes**
24 **represent the first stage of the back-arc Adria continental breakup in Permian. During the Palaeotethys-**
25 **Adria collision, underplating controlled topography and palaeogeographic domains resulting in the**
26 **observed asymmetrical sedimentary evolution since Triassic across the Adria microplate. Finally, we**
27 **propose that the Palaeotethys-Adria boundary in Permian was similar to the actual Pacific-Okhotsk plate**
28 **boundary.**

29

30 The Adria plate today extends along the Adriatic Sea from the Po plain to the Apulian promontory and is
31 surrounded by the Alpine, Dinaric and Apenninic orogens to the north, east and west, respectively (Figure
32 1a). There are evidences suggesting that the Adria plate may be fragmented in two microplates, the Adria
33 *sensu stricto* (s.str.) to the north and the Apulia s.str. to the south (Oldow et al., 2002; D'Agostino et al.,
34 2008; Handy et al., 2019) but if this division has developed in recent times or if it was inherited from older
35 epochs is unclear. Mesozoic and Cenozoic evolution of the Adria plate is related to a wider geodynamic

36 setting involving the African and the Eurasian Plates whose relative motions allowed for the observed
37 counterclockwise rotation of the plate since Cretaceous (Bennett et al., 2008; Faccenna et al., 2014). In
38 Permian times this area was located in the northernmost pivot of the Palaeotethys, in a region supposed to
39 have undergone wide continental extension related to the opening of the Palaeotethys ocean and, during
40 late Permian and Trias, of the Neotethys to the west (Moix et al., 2008; Stampfli and Hochard, 2009;
41 Stampfli et al., 2013). To date however, evidences of the ancient Adria s.str. oceanic crust are missing
42 across the entire plate from the Dinarides to the Apennines (Sun et al., 2019; van Unen et al., 2019).

43 Despite the actual tight setting, locations of the boundaries between the Adria plate and the surrounding
44 plates are still matter of debate (Anderson and Jackson, 1987; Stampfli and Hochard, 2009; Stein and Sella,
45 2005), while several evidences (Herak, 1986; Moretti and Royden, 1988; Doglioni et al., 1994; Tari, 2002;
46 Bennett et al., 2008; Korbar, 2009; Faccenna et al., 2014; Mancinelli et al., 2018; Sun et al., 2019) suggest
47 that Adria is subducting both beneath the Dinaric and the Apenninic belts. The Central Adriatic Sea is
48 geographically surrounded by Permian and Triassic volcanism that is outcropping or has been drilled by
49 explorative boreholes. These events are distinguished in two major episodes, on one side there are
50 evidences of scattered Neotethys-related volcanism between Late Permian and Middle Triassic in the Po
51 Plain, Northern Adriatic, Istria Peninsula, Dinarides and Apulian Peninsula (Buser, 1987; Tari, 2002; Velić et
52 al, 2002; Pamic and Balen, 2005; Bernoulli, 2007; Cassinis et al., 2008; Gaetani, 2010; Scisciani and
53 Esestime, 2017), while in Southern Alps there are evidences of wide intrusive and effusive bodies related to
54 the subduction of Palaeotethys ocean beneath Eurasia in Permian (Cassinis et al., 2012). Moreover, a
55 Permian underplating event was associated to post-Hercynian outcrops across the European Alps (Schuster
56 and Stüwe, 2008).

57 Some clues about the early history of the Adria plate are preserved in the Croatian archipelago where
58 gabbroic intrusions are found on the Jabuka and Brusnik islets (Balogh et al., 1994; Juracic et al., 2004;
59 Pamic and Balen, 2005; Palinkaš et al., 2010). Targeted by several datings during the years, the estimated
60 age of these gabbroic intrusions has ranged between 200 and 273 ± 1.1 My with latter dating (Palinkaš et
61 al., 2010) supporting the older age together with later reworking of the gabbros of Jabuka at 77 ± 2.4 My.

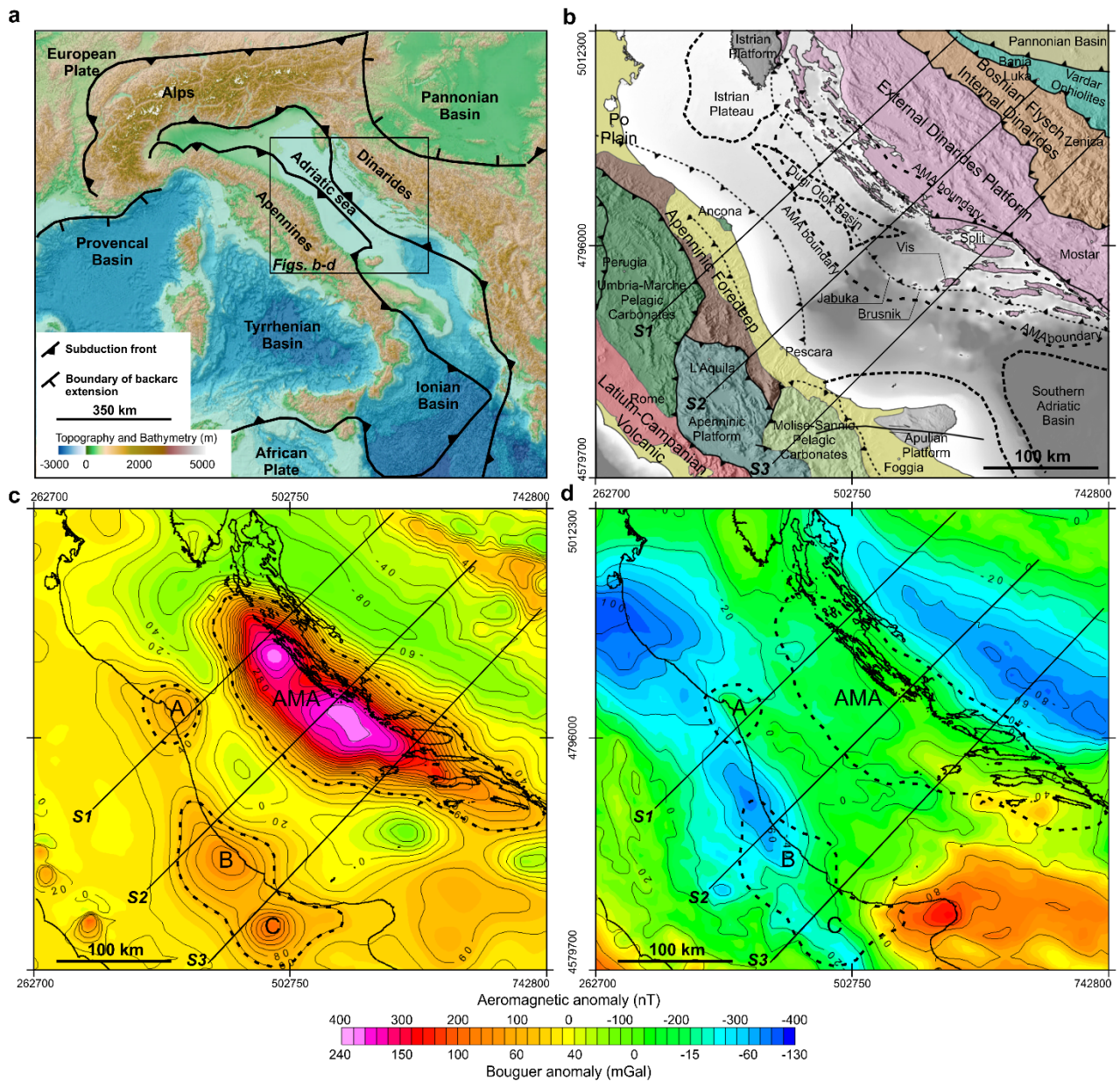
62 Two main questions arise from these outcrops in the Croatian archipelago: are these evidences
63 representative of some larger-scale event? And how do these gabbroic intrusions survived in this complex
64 geodynamic scenario?

65 Several authors attempted in the last years to answer these questions through several efforts focused on
66 the analysis and modeling of the Adriatic Magnetic Anomaly (AMA, Figure 1b-d). The AMA represents the
67 most prominent feature within the Adria plate due to the paucity of seismicity with respect to the
68 neighboring chains (Faccenna et al., 2014; Sun et al., 2019) and its moderate average crustal thickness (~ 30
69 km – Nicolich, 2001; Sumanovac, 2010; Tassis et al., 2013). The first evidence of a ~ 100 km-wide and ~ 400

70 km-long AMA was provided by the aeromagnetic map of Italy (Chiappini et al., 2000; Caratori Tontini et al.,
71 2004). Later, the dataset was extended towards the Croatian onshore by Giori et al. (2007) producing a
72 larger coverage but still incomplete map over the AMA that was used to support a regional-scale source
73 rather than local smaller sources (Mancinelli et al., 2015). These findings, despite based on incomplete data
74 coverage, were later validated by inverse modeling over a full-coverage map (Milano and Fedi, 2016).

75 At full data coverage, the AMA extends over 200 km in the SW-NE direction and 400 km in the NW-SE
76 direction along the Adriatic Sea with maximum anomaly values of ~ 370 nT (Milano and Fedi, 2016). When
77 observed at regularly-spaced color intervals the AMA shows two main peaks (Figure 1c) and a straight NW-
78 SE boundary along the Croatian onshore-offshore transition with a negative anomaly area still trending
79 NW-SE in the Croatian and Bosnia and Herzegovina onshore. Conversely, the southwestern boundary is
80 arcuate with a trend ranging N-S to W-E from north to south of the boundary. In the southwestern Central
81 Adriatic the magnetic anomaly is alternatively mapped by positive and negative spots while more towards
82 southwest, on the Italian shoreline and onshore areas, three main highs (A, B and C) are found (Figure 1c).
83 The AMA results with clear and sharp northern and eastern boundaries while the western and southern
84 boundaries are less obvious and possibly blurred with surrounding anomalies. The AMA locates the only
85 clearly observable signal at satellite altitude over Southern Europe (Milano et al., 2019) and thus it certainly
86 represents a deep and regional-scale phenomena that is related to the geodynamic evolution of the Adria
87 plate and whose source cannot be limited to the outcropping gabbroic intrusions. To date however, the
88 geodynamic context that led to the emplacement of the causative source of the AMA was never
89 investigated. Similarly, eventual relations between the AMA and the A-C surrounding positive anomalies
90 were never investigated despite some authors (Minelli et al., 2018; Mancinelli et al., 2019) suggested that
91 the B anomaly is related to high magnetic susceptibility (~ 0.05 SI units) sources at the base of the crust.

92



93

94 **Figure 1** Geodynamic, geological and geophysical characters of the Central Adriatic Sea and surroundings.

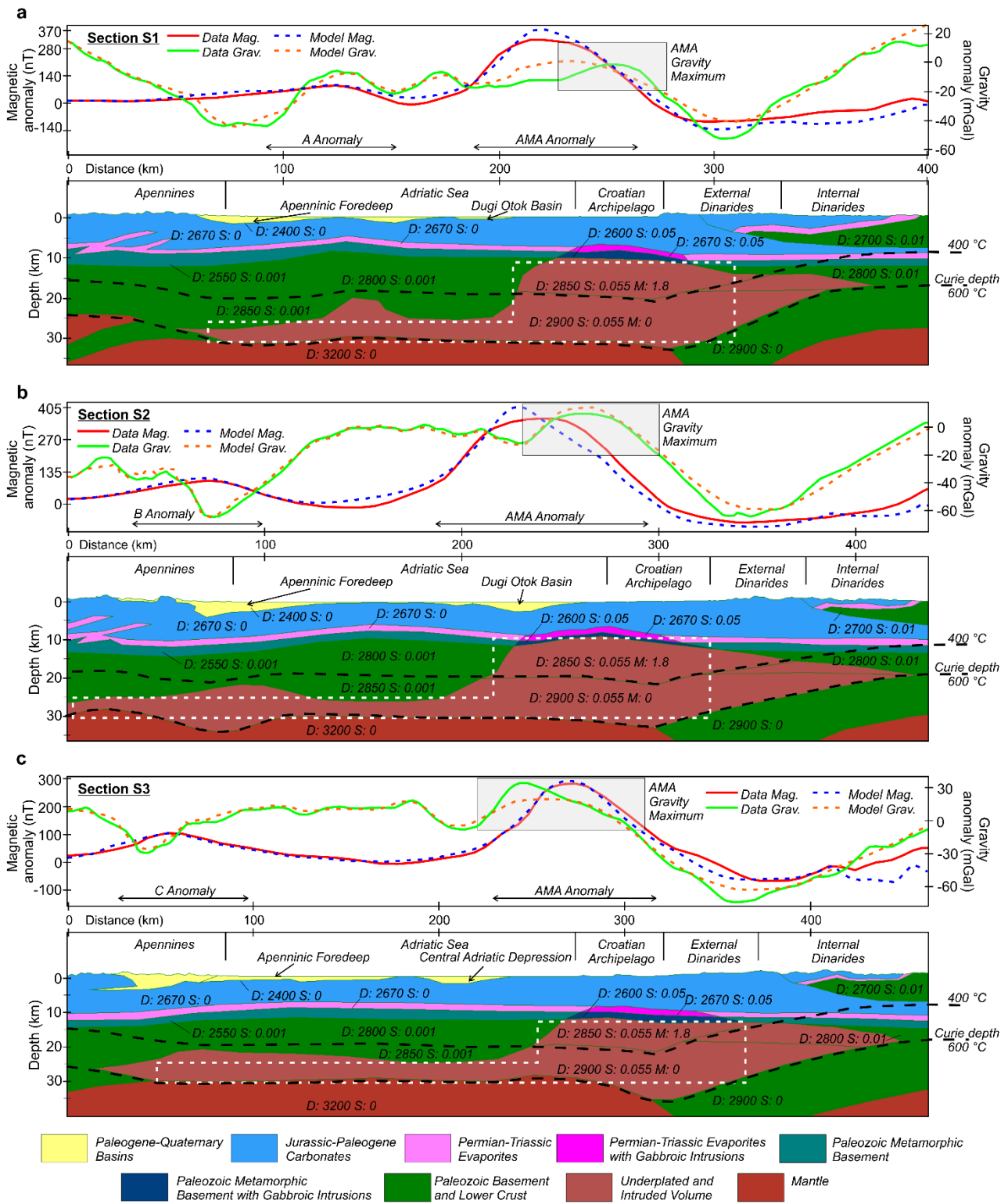
95 **a**, Actual geodynamic settings of the Central Mediterranean Sea and location of the study area. **b**,
 96 Simplified geological sketch map over the Central Adriatic Sea, Apennines and Dinarides (CNR – PFG, 1991;
 97 van Unen et al., 2019). **c**, Aeromagnetic anomaly at 2500 m height showing the AMA and A-C positive
 98 anomalies after Caratori Tontini et al. (2004) and Milano and Fedi (2016). AMA peaks are centered at
 99 486000 E, 4873000 N and 557000 E, 4812000 N. Anomaly A is centered at 395000 E, 4825000 N (~85 nT)
 100 few km offshore the Ancona promontory; anomaly B is centered at 442000 E, 4681000 N (~130 nT) and
 101 anomaly C is centered at 483000 E, 4617000 N on the Abruzzo-Molise onshore. These three highs in the
 102 Apenninic foreland domain are relatively closer to the AMA from south to north with maximum and
 103 minimum distances along the SW-NE direction of ~200 and 100 km. **d**, Bouguer anomaly over the modeled
 104 area (reduction density of 2670 kg m^{-3}) after Tassis et al. (2013) and data over Italy and surroundings (CNR –
 105 PFG, 1991). When compared with the Bouguer gravity map over the area, the AMA northeastern boundary
 106 clearly relates to the boundary of the NW-SE Bouguer gravity minimum mapped over Dinarides, while all
 107 the other AMA boundaries do not match with gravity highs or lows. Black continuous lines in b-d locate the
 108 modeled sections (S1-S3). Coordinates in this and following figures are in UTM33N WGS84.

109

110 Available deep seismic data across the area are limited to the CROsta Profonda (CROP) profiles (Scrocca et
111 al., 2003) that across the Adriatic Sea generally show poor data quality below 7 s two-way-time (TWT) with
112 an exception given by CROP M17C crossing the area NNW-SSE (Figure S1). Several other commercial
113 seismic profiles were acquired for hydrocarbon prospection but these were always limited in depth to 6 or
114 7 s TWT. Similarly, tens of boreholes were drilled in the Central Adriatic Sea for exploration purposes but
115 these never reached the pre-Permian sedimentary sequences across the entire Central Adriatic Sea
116 (Scisciani and Esetime, 2017).

117 To address the open questions about the AMA and provide a plausible geodynamic interpretation of the
118 causative source, we forward model the observed aeromagnetic anomaly and Bouguer gravity along three
119 SW-NE trending ~400 km-long sections extending from the onshore Central Italy through the Adriatic Sea,
120 onshore Croatia and Bosnia and Herzegovina (S1-S3 in Figures 1 and 2).

121



122

123 **Figure 2. Forward modeling of the S1-S3 sections.** **a**, Magnetic and gravity anomalies forward modeling
 124 across section S1. **b**, Magnetic and gravity anomalies forward modeling across section S2. **c**, Magnetic and gravity anomalies forward modeling across section S3. Modeled density (D) and magnetic susceptibility (S)
 125 and gravity anomalies forward modeling across section S3. Modeled density (D) and magnetic susceptibility (S)
 126 values are indicated for each body. Remanent magnetization (M) is assigned only to high susceptibility
 127 volumes above the 400 °C isotherm (see methods section). Areas bounded by white dashed lines locate are
 128 those considered for estimation of the volume of the magnetic sources (see methods section). Vertical-to-
 129 horizontal scale ratio across the modeled sections is 0.5. Reference starting values for the Moho depth
 130 across the modeled area are from literature (Scarascia et al., 1998; Sumanovac, 2010; Tassis et al., 2013).

131

132 The modeled sources extend upwards from the Moho discontinuity through the crust with higher density
133 and magnetic susceptibility (≥ 0.05 SI units) than the surrounding volumes. The modeled susceptibility
134 values are comparable to those related to deep sources in Central Apennines (Minelli et al., 2018;
135 Mancinelli et al., 2019). Minimum thicknesses of the sources are observed toward model ends, both NE and
136 SW, and beneath the Central Adriatic Sea. However, lateral continuity is never interrupted along all the
137 three models. The shape of the magnetic sources results coherently from the modeled sections in the form
138 of an asymmetric crustal batholith whose basal layer widens southwards (Figure 2a-c). The thickness of the
139 source increases northeastwards to maximum values of ~ 20 km along sections S1 and S2 beneath the
140 Croatian archipelago, while its lateral extent ranges between 250 and 400 km from north to south. Beneath
141 the Dinaric belt, the modeled AMA source base is at ~ 20 km depth due to shallower Curie isotherm (see
142 methods section) but we can speculate that also the volumes constituting the crustal root of the Dinarides
143 may have undergone the same processes because the modeled density values fit the AMA source density.
144 The AMA source is laterally asymmetric also considering its upper bound because in the Dinaric domain the
145 top of the source propagates to depths significantly shallower than in the Adriatic domain (Figure 2). Given
146 the evidences of significant volume transfer from Adria to Dinarides during their Eocene-to-present
147 collision (Bennett et al., 2008), we speculate that this asymmetry is representative of tectonic reworking of
148 the AMA source during the Adria-Eurasia collision.

149 In the upper crust, the AMA source propagates with gabbroic intrusions through the basement and the
150 sedimentary cover reaching a minimum depth of 9 km within the Triassic evaporites NE of the Dugi Otok
151 depression along section 2 (Figure 2b). This suggests that the Triassic evaporites postdated the AMA
152 source, whose emplacement probably occurred before mid-late Permian age. Thus, our modeling supports
153 the latter dating of the gabbroic intrusions on Jabuka and Brusnik islets (Palinkaš et al., 2010) rather than
154 previous estimates proposing younger ages. The gabbros outcropping in these islands were later exhumed
155 by compressional and transpressional tectonics (Tari, 2002) related to the Dinaric chain emplacement.

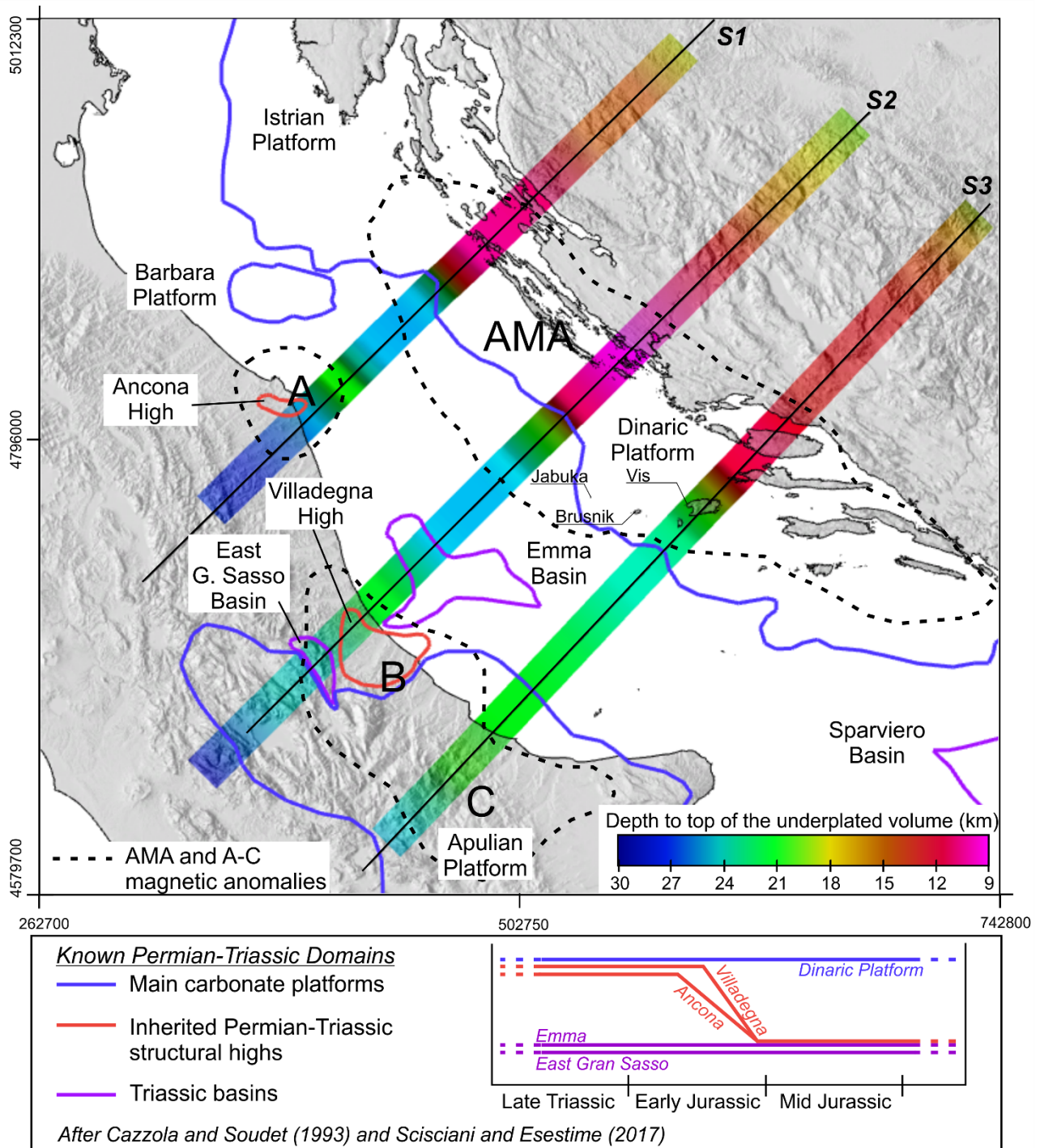
156 The observed magnetic anomalies over the Central Adriatic Sea and surroundings are thus prevalently
157 related to deep sources with small contributions from low susceptibility lower crust and basement. Given
158 the spatial distribution at the base of the crust and the magnetic susceptibility of the modeled bodies,
159 these sources are interpreted as massive underplated and intruded gabbros beneath the Adria s.str.
160 microplate. This view is also supported by the Bouguer gravity anomaly because local maximums of the
161 observed gravity are found over the AMA in all the modeled sections (Figure 2a-c) suggesting that the
162 cooling of the underplated and intruded material has increased also the density of the lower crust. If our
163 interpretation is correct, the modeling provides an estimate of the longitudinal extent of the underplated
164 material that may range up to ~ 400 km. Furthermore, the modeled sections suggest that given its volume

165 and extent, the underplated material represents an episode of massive and large-scale magmatic activity of
166 Permian affinity rather than Triassic (Cassinis et al., 2012).

167 A conservative estimate of the volume of the modeled high-susceptibility sources (see methods section)
168 provides a value of $\sim 0.5 \times 10^6 \text{ km}^3$. This volume encompasses both the underplated and intruded material
169 and accounts also for the small portions of the upper crustal volumes hosting the shallow magmatic
170 intrusions within the basement and early Triassic succession.

171 Considering the volume of the batholith and intruded gabbros as resulting from the modeling and its
172 transparency as shown in deep seismic profiles imaging in the area (figure S1), we can speculate that after
173 the underplated and intruded material was supplied, it undergone a long-lasting cooling and solidification
174 period (Thybo and Artemieva, 2013). This implies that in the Adria s.str. area the continental breakup never
175 evolved to oceanic spreading with new crust formation but it aborted soon after the first underplating
176 phase, following an evolution similar to that proposed for the Permian igneous and metamorphic rocks in
177 the European Alps by Schuster and Stüwe (2008). This supposed interruption of the breakup evolution is
178 supported by the lacking of volcanic evidences from outcrops and boreholes in the entire Central Adriatic
179 Sea because short timings ($< 0.1 \text{ Ma}$) are required between underplating and the following magmatism
180 (Petford et al., 2000; Thybo and Artemieva, 2013). However, we suggest that some consequences of the
181 aborted rift in the Central Adriatic Sea are still evident.

182 In figure 3 we compare the top of the underplated and intruded volumes against the distribution of known
183 long-lasting carbonate platforms and Permo-Triassic structural highs in Central Adriatic and surroundings.
184 These regions locate palaeogeographical scenarios that never evolved to slope or basin domains during
185 Jurassic or Cretaceous times (Dinaric platform) or made their transition during Triassic or Jurassic, with
186 significant delay when compared to surrounding depositional sequences. Among the latter, we include the
187 Ancona and Villadegna highs where stratigraphic evidences (Cazzola and Soudet, 1993; Scisciani and
188 Esestime, 2017) suggest that palaeogeographical domains during Triassic and early Jurassic were
189 tectonically controlled. In these areas, the uplifted regions allowed for longer-living shallow water
190 environments while these were surrounded by deeper conditions such as the Emma and the East Gran
191 Sasso basins located east and west of the Villadegna area, respectively (Scisciani and Esestime, 2017). In the
192 case of anomaly C such evidences are buried beneath $\sim 12 \text{ km}$ of overlying Apulian platform and Southern
193 Apennines foredeep deposits (Butler et al., 2004) that cover the westward-subducting Adria crust and
194 prevents any detection of eventual Permian uplift of Adriatic affinity.



195

196 **Figure 3. Comparison between the modeled underplated volume and known Adria Permian-Triassic**
 197 **domains.** The spatial trend of the top of the underplated volume (color-coded bands) is compared against
 198 the boundaries of the mapped magnetic anomalies (dashed black lines) and the spatial distribution of the
 199 known palaeogeographical domains in late Permian-early Triassic (color-coded lines). The drowning timing
 200 of the inherited structural highs is also provided in the lower plot and compared to surrounding basins and
 201 Dinaric platform. The north-eastern areas where shallower magnetic sources are found along modeled
 202 sections S1 and S2, matches the boundary of the long-living Dinaric carbonate platform. The south-western
 203 areas below the A-C anomalies correspond to inherited structural highs from Permian uplifted regions (A
 204 and B) and to a region of Adriatic affinity beneath the Apulian platform and Southern Apennines foredeep
 205 (C).

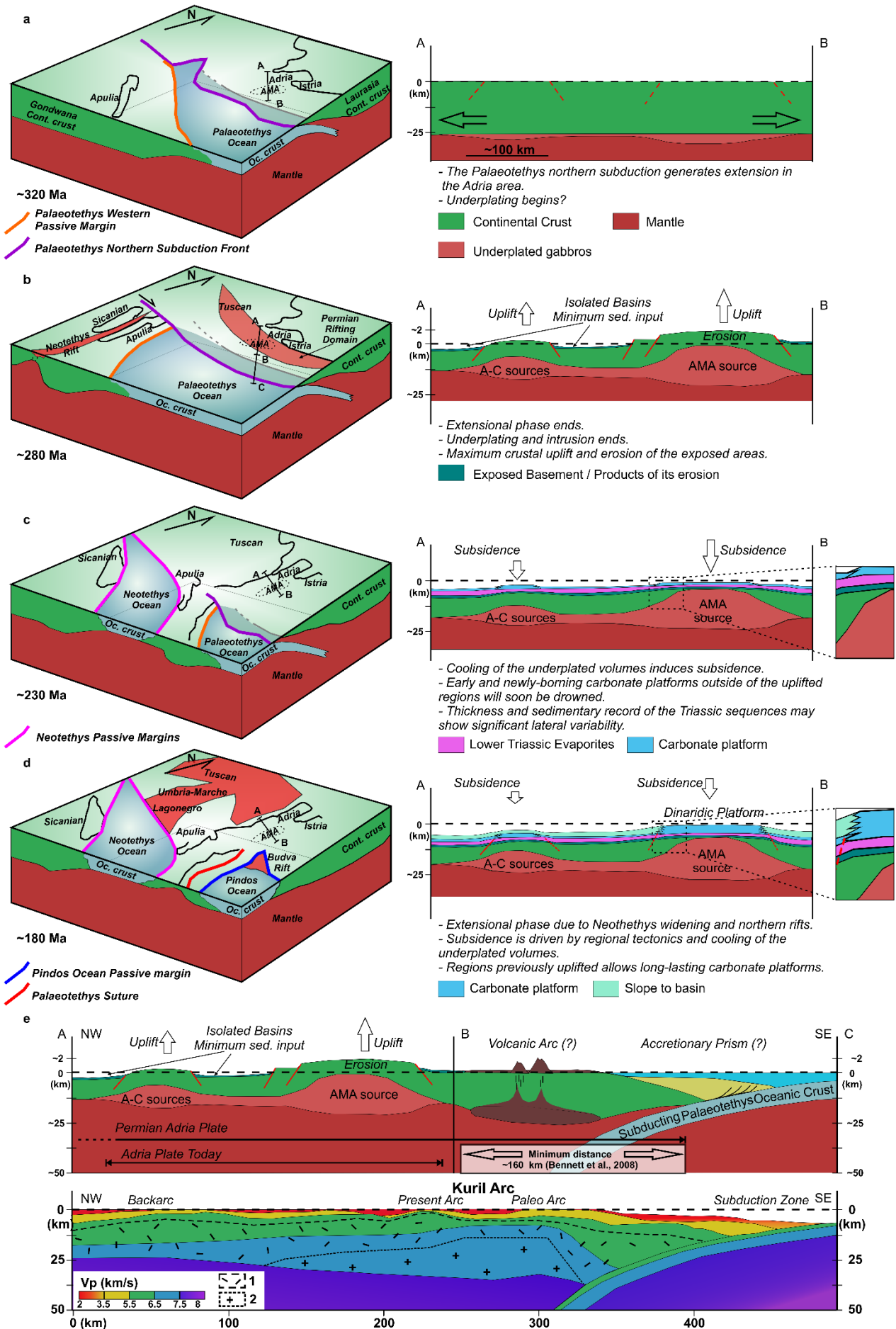
206

207 The fitting between the modeled deep crustal magnetic source and these regions is surprising and
208 intriguing. Considering the spatial distribution of such domains and the marked asymmetry across Central
209 Adriatic given by the thick and continuous Dinaric platform (Scisciani and Esetime, 2017) compared to the
210 scattered structural highs and basins in the Western Adriatic area, we speculate that the causes for such
211 evidences are related to regional-scale phenomena affecting the tectonic setting of the upper crust.
212 Furthermore, we suggest that the observed heterogeneity in the palaeogeographical Permian domains is a
213 direct consequence of the underplated and intruded material that over-compensated the rift-related
214 crustal thinning resulting in uplifted regions of crust corresponding to major underplated volumes (figure
215 4a-b).

216 The basement that was exhumed because of the underplating was eroded during Permian allowing the
217 intruded gabbros in the basement to further shallow. Possibly, thanks to later tectonic reworking and uplift,
218 these small and shallower volumes are those outcropping in the Croatian archipelago. After an evaporitic
219 sedimentation phase in Lower Triassic, whose products show heterogeneous thickness and distribution
220 across the area (figure 4c; Scisciani and Esetime, 2017), carbonate platforms lasted longer in the uplifted
221 regions and were preserved since Cretaceous with respect to the surrounding regions where marginal and
222 basin conditions rapidly developed since late Triassic (figure 4c-d). Such heterogeneous scenario implies
223 that the flexural strength of the crust was very low or null, a view that is compatible with the continental
224 breakup phase and the related crustal thermal regime.

225 In figure 4e we propose an interpretative view of the Palaeotethys-Adria s.str. boundary in Permian
226 suggesting that this collisional margin was similar to the actual Pacific-Okhotsk plate boundary where
227 underplating contributes to crustal accretion beneath and behind the Kuril arc (Nakanishi et al., 2009;
228 Thybo and Artemieva, 2013). In this scenario, the minimum distance between the AMA anomaly and the
229 Permian Palaeotethys subduction front was ~150 km (figure 4e). This spatial reference is compatible with
230 the proposed collisional scheme and with the regional palaeogeographic Permian scenario (Stampfli et al.,
231 2013). Moreover, this interpretation is further supported by the depth (~160 km) reached by the subducted
232 Adria slab beneath Dinarides during their Eocene-to-present collision (Bennett et al., 2008).

233



235 **Figure 4 Conceptual models of the formation and Permian-Jurassic evolution of the underplated gabbros.**
236 **a**, Late Carboniferous palinspastic sketch illustrating the Adria s.str. and Apulia s.str. microplates and
237 surroundings; due to the inception of back-arc spreading the underplating possibly started during the
238 widening of the Palaeotethys Ocean. **b**, During Permian times the increasing underplated volume provides
239 substantial uplift in the areas where the major volumes are localized. In Mid Permian, the opening of the
240 Neothethys western branch stops the underplating and prevents breakup completion. Sedimentation in
241 internal basins is limited and localized, mostly consisting of erosional products of the exposed basement. **c**,
242 In a period of tectonic stasis due to the closing of the northern Palaeotethys branch, post-underplating
243 subsidence has produced its effects and Triassic evaporites are deposited above the basement. **d**, During
244 Late Triassic and Lower Jurassic the regions that undergone higher uplifts in the previous period allow the
245 Dinaric carbonate platform to grow longer, while in adjacent areas slope and deeper environments are
246 found. The opening of the Umbria-Marche and Lagonegro basins is lateral (westwards) to the Adria s.str.
247 microplate but likely contributes to tectonic subsidence of the western Adria basins. **e**, Regional model
248 section across the subducting Palaeotethys oceanic crust and the study area during Permian (for location
249 see [figure 4b](#)) compared with the P-wave velocity model across the Kuril arc (Nakanishi et al., 2009) and its
250 interpretation – 1: Post-fractionation and delaminated underplating; 2: Mafic underplating (Thybo and
251 Artemieva, 2013). Palaeogeographic maps are modified after Moix et al. (2008), Stampfli and Hochard
252 (2009), Stampfli et al. (2013).

253

254 Assuming an Airy-type response within the crust (Watts, 2001) we can estimate ([see methods section](#)) the
255 maximum uplift induced by the underplating load to be ~ 2000 m in the Dinaric domain. This estimate is
256 supported by the differential growth of the Dinaric platform in respect to the Adriatic domain. In the first
257 case, above the thicker and wider AMA source, we find a wide and continuous Dinaric carbonate platform
258 lasting from Late Triassic to Paleogene (Scisciani and Esetime, 2017). In the Adriatic domain, above the
259 thinner sources that we interpret as causative of the A and B anomalies, we find scattered duration of the
260 carbonate platforms and structural highs ([Figure 3](#)) whose spatial distribution coincides with locations of
261 the A and B anomalies and causative sources. The drowning of these latter domains was likely driven by
262 faster cooling of the thinner underplated material accelerating upper crustal subsidence (Schuster and
263 Stüwe, 2008) with possible later contributions from the western Jurassic rifting systems ([Figure 3d](#)).

264 In this framework, strong magnetic sources are lacking at the base of the southernmost Apulian s.str. crust
265 ([Figure 1c](#); Caratori Tontini et al., 2004; Milano and Fedi, 2016) because during Permian times the Apulia
266 s.str. microplate pertained to the Cimmerian terranes and was in between the Palaeotethys and the newly-
267 opening Neothethys (Stampfli et al., 2013), away from the Adria underplating ([Figure 4b](#)). If the Apulian
268 promontory was in the same position relative to the Adriatic Sea as today, it should testify this with
269 magnetic signatures like those found in the Central Adriatic Sea ([Figure 1](#)) and/or with massive Permian
270 magmatic intrusions like those observed in the Alps (Cassinis et al., 2012) or resulting from our models.
271 Such evidences are lacking because only one thin level of volcanic deposits is found interlayered in shallow-
272 water carbonates of Apulian affinity across the complete Permian sequence drilled by the Gargano 1
273 borehole (Scisciani and Esetime, 2017). On the contrary, the C anomaly is apparently related to the

274 Apulian platform (Figure 3) but it is actually related to the Permian underplating beneath the Adria s.str.
275 microplate and thus pertains to the westward-subducting Adria s.str. crust.

276 Geometries of the modeled volumes may suggest a tectonic underplating process (Menant et al., 2019)
277 related to the Palaeotethys subduction beneath the Permian Adria. In this scenario, the outcropping
278 gabbros and the underplated volume would represent the lower Palaeotethys oceanic crust tectonically
279 stacked during its subduction beneath Adria. Despite the observed topographic uplift seems to support this
280 view (Menant et al., 2020), a tectonic origin for the underplating can be ruled out because of the timing,
281 thickness and gabbroic nature of the underplated material. In fact, the ~20 km thick gabbroic volumes are
282 significantly younger than the Palaeotethys oceanic crust. Furthermore, the thin and deep gabbroic oceanic
283 crust is not involved by tectonic stacking that should allow underplating only of the upper basaltic layers
284 (Menant et al., 2019) that are missing across the entire study area.

285 An alternative view could regard the AMA source as a fossil seamount pertaining to the Palaeotethys ocean
286 that was exposed by erosion of the accretionary prism once the Palaeotethys was closed. The size of the
287 AMA source is compatible with other cases along the Palaeotethys suture (Moix et al., 2008; Federici et al.,
288 2010; Moix et al., 2013; Eyuboglu et al., 2018) but the basaltic, ophiolitic and metamorphic facies that
289 usually are found in such cases are missing in the Central Adriatic area. Moreover, a seamount origin for the
290 outcropping gabbros is further discredited by their trace element concentration that supports an Island-Arc
291 origin (Figure S2).

292 Another plausible alternative scenario can relate the AMA underplating to the northwestern termination of
293 the Pindos ocean – i.e. the Budva rift (Stampfli and Kozur, 2006; Moix et al., 2008). Given the Budva-Adria
294 s.str. proximity in Late Triassic-Early Jurassic times (figure 4), if the Budva rift survived to the Pindos
295 subduction, its attenuated lithosphere may have carried the AMA underplated gabbros towards the
296 external Dinarides during later transcurrent deformation (Stampfli and Kozur, 2006). In such case however,
297 the AMA anomaly and its causative source should locate at least in the external Dinarides or, given the
298 Cenozoic Adria-Eurasia collision, it should be even more internal on the Dinaric chain. Furthermore, this
299 hypothesis is not matched by the Triassic evaporites postdating the underplated gabbros as resulting from
300 our modeling (figure 2).

301 Finally, we propose that the emplacement of the underplated material is related to the Palaeotethys-Adria
302 s.str. convergence in the form of a back-arc extension (Figure 4e). Such scenario was common in the
303 northern Palaeotethys margin (Stampfli et al., 2004) due to the acceleration of Palaeotethys slab rollback
304 after the end of Gondwana and Laurasia convergence and collapse of the Laurasian active margin (Vavassiri
305 et al., 2000). The back-arc regions firstly evolved towards shallowing or exhumation of the lower crust over
306 large areas (including the Adria s.str. region) in a Basin and Range fashion (Zandt et al., 1995), and finally

307 towards opening of the small Triassic back-arc oceans (Meliata, Maliak, Pindos-Huglu) (Stampfli and Kozur,
308 2006).

309 If this rifting was completed laterally (southwards) to the Adria s.str. microplate or if it evolved
310 discontinuously and completion of the breakup was aborted only in this region remains unclear. However,
311 in the first case the evidences would have been consumed by the Adria subduction beneath Dinarides,
312 whilst in the second case this portion of the Adria s.str. microplate was very close to formation of new
313 oceanic crust, as testified by intrusive bodies reaching shallow depths, but in late Permian-early Triassic a
314 rapid change in the geodynamic context has stopped rift completion. We suggest that this event is the
315 opening of the northwesternmost Neotethys branch that sets the stage to close the gap between the
316 Apulia s.str. and Adria s.str. microplates to form the wider Adria as it is today, accelerates the closure of the
317 Palaeotethys ocean and stops the extensional tectonics in the Adria s.str. area (Figure 4c-d).

318 If the linkage between the AMA source and the sources of the A- C anomalies is accepted, then some
319 constraints are provided to the extent of the Adria s.str. microplate. In fact, the boundary between Adria
320 s.str. and Apulia s.str. should be located south of the C anomaly. In this area surrounding the Gargano
321 promontory the lithosphere thickens southwards (Calcagnile and Panza, 1981) and broad E-W transform
322 deformation was related to inherited discontinuities in the deep crust (Di Bucci et al., 2006). Furthermore, a
323 significant GPS velocity increase was observed between the areas north and south of the Gargano
324 promontory (Oldow et al., 2002) and recent findings suggest that the Adria plate as intended today
325 extending from the Alps to the Apulian promontory, is fragmented in two subplates rotating in opposite
326 directions and whose boundaries are located in the Gargano promontory area (Handy et al., 2019). We
327 interpret all these features as indicative of the boundary between the Adria s.str. and Apulia s.str. grossly
328 corresponding with the E-W transform zone, but whose eventual upper crustal evidences were masked by
329 the Cenozoic Apenninic orogenesis. In this view, this area locates a Mesozoic plate boundary that is still
330 affecting the geodynamic evolution of the area.

331 The case of the Adria plate demonstrates that underplating processes in collisional dynamics may
332 contribute to continental crust accretion and, in the long term, to preserve crustal thickness. This is the
333 case in the Pacific-Okhotsk plate boundary as it was in the Palaeotethys-Adria s.str. collision. Underplating
334 contribution is showcased by the long-living Dinaric platform whose evolution since Permian times would
335 have been completely different without the underplated volume that, by providing significant uplift and
336 crustal buoyancy, has controlled the topography/bathymetry ultimately allowing for platform growth and
337 palaeogeographic differentiation. In the long-term evolution of the plate, the underplated volume has
338 probably played a key role also in the Adria-Eurasia collision by partial transfer of crustal volumes from the
339 Adria plate to the Dinaric belt.

340

341 **Methods**

342 **Forward modeling of the magnetic anomaly**

343 In our modeling, we set a maximum magnetic susceptibility threshold of 0.05 ± 0.005 (SI units) compatibly
344 with estimates from Minelli et al. (2018) and modeling in the Central Apennines by Mancinelli et al. (2019).
345 All the other bodies modeled across the sections were given susceptibility values ranging between 0 and
346 0.055 SI units.

347 A fundamental constraint when modeling magnetic anomalies is given by the Curie isotherm. Here, we set
348 a magnetite Curie temperature of 600 °C (Frost and Shive, 1986; Shive et al., 1992). To locate the Curie
349 isotherm we assume an average crustal thermal conductivity of $2.5 \text{ W m}^{-1} \text{ K}^{-1}$ (Turcotte and Schubert, 2002;
350 Pauselli et al., 2006; Pauselli and Ranalli, 2017) and calculate the conductive thermal gradient using heat
351 flow data from Central Italy (Pauselli et al., 2019), the Adriatic Sea (Della Vedova et al., 2001) and heat flow
352 values from Bosnia and Herzegovina (Atlas of geothermal resources in Europe, 2002). We also use thermal
353 gradient data over Croatia (Kurevija et al., 2014).

354 The observed conductive heat flow (q) is given by:

$$355 \quad q = -k \frac{\partial T}{\partial Z}$$

356 where k is the thermal conductivity of crustal rocks and $\partial T/\partial Z$ is the thermal gradient (Fourier, 1822).

357 The resulting Curie depth is estimated to range between 35-40 km in the Apenninic and Adriatic areas,
358 where lower heat flow values ($30\text{-}40 \text{ mW m}^{-2}$) are observed, and ~ 20 km in the northeastern part of the
359 investigated area of Bosnia and Herzegovina, where the highest thermal gradient (30 K km^{-1}) and heat flow
360 values ($\sim 75 \text{ mW m}^{-2}$) are found. Considering that the Moho discontinuity represents a magnetic boundary
361 preventing any contribution from the mantle to generate anomalies (Wasilewski et al., 1979; Wasilewski
362 and Mayhew, 1992), these estimates allow to assume that the observed magnetic anomalies may come
363 from sources located within the entire crust in the Apenninic, Adriatic and Croatian onshore domains, while
364 sources in the northeastern area are located within the upper crust.

365 For the modeling we set the following parameters of the magnetic field: field intensity (H) 36.8 A/m ,
366 inclination (I) 58° , declination (D) -0.1° . In modeling the magnetic anomalies we consider both induced
367 (M_i) and remanent magnetization (M_r). The first is attributed to each body above the Curie depth through
368 the magnetic susceptibility ($M_i = S \times H$). The remanent magnetization is attributed only to large underplated
369 volumes above the 400°C isotherm because at higher temperatures M_r contributions are unlikely due to its
370 unstable and viscous signature (Pullaiah et al., 1975; Schlinger, 1985; Minelli et al., 2018). Given the
371 uncertainties about magnetization values of the underplated gabbros (Bronner et al., 2011), we assume an

372 effective average M_r value of 1.8 A m^{-1} with a magnetization vector inclination of 0° and declination of 12°
373 according to the Permian paleopole (Van der Voo, 1990).

374 The high magnetic susceptibilities used to model the main sources of the AMA and surrounding magnetic
375 anomalies exclude the possibility of a granitic composition for these bodies (Punturo et al., 2017) and are
376 similar to susceptibility values observed on samples from the Ivrea-Verbano area (Rochette, 1994).

377 **Volume estimates of the magnetic anomalies sources**

378 To estimate the volume of the causative source for the observed magnetic anomalies we use the minimum
379 values of thickness and lateral extent (SW-NE direction) of the source as resulting from the modeled
380 sections (white dashed squares in **figure 2**). Furthermore, we consider the distance between section 1 and
381 3 ($\sim 180 \text{ km}$) to represent the third dimension of the source along the NW-SE direction. Only volumes with
382 magnetic susceptibility ≥ 0.05 (SI units) are considered. From the volume estimate we exclude the volumes
383 outside the white dashed boxes in **figure 2** – i.e. the northernmost wedge-shaped anomalous sources and
384 the A-C sources, due to their marked lateral variability. This approach provides a conservative estimate of
385 the AMA source volume ($0.3 \times 10^6 \text{ km}^3$) and of the underplated material beneath the Adriatic Sea and Italian
386 onshore ($0.2 \times 10^6 \text{ km}^3$). Throughout the text, when we refer to sources we imply both the AMA and the
387 Western Adriatic Sea and Italian onshore sources related to the A-C positive anomalies.

388 **Uplift estimates caused by underplating**

389 Uplift estimate is produced assuming an Airy-type response of the crust to the underplating load (see text
390 for discussion) given by

$$391 \quad u = v \frac{(\rho_m - \rho_x)}{(\rho_m - \rho_w)}$$

392 Where u is the induced uplift, v is the thickness of the underplated body, ρ_m is the density of the mantle
393 (3200 kg m^{-3}), ρ_x is the density of the underplated body (2900 kg m^{-3}) and ρ_w is the density of water (1030
394 kg m^{-3}) (Watts, 2001). **Table 1** shows the estimated uplift due to underplated material thickness ranging
395 between 2 and 25 km. If a regional uplift is assumed to be $\sim 700 \text{ m}$ due to the basal layer of the source
396 averaging 5 km thickness in all the modeled sections, the maximum uplift beneath the AMA source ranges
397 between 2700 and 2000 m for underplating thickness of 25 and 20 km, respectively. Above the sources for
398 the A-C anomalies in Western Adriatic Sea and onshore Italy, the maximum estimated uplift is $\sim 700 \text{ m}$
399 because of the average underplating thickness of 10 km across all modeled sections (**Figure 2**).

v (km)	2	5	10	15	20	25
u (m)	276	691	1382	2074	2765	3456

400 **Table 1.** Airy-type crustal uplift u (m) compared to the thickness of the causative underplated material v
401 (km).

402

403 **Acknowledgments and data availability**

404 All the data used in this work are available from literature and published maps.

405 **Authors contributions**

406

407 **Competing interests**

408 The authors declare no competing interests.

- 410 1. Anderson, H. A. and Jackson J. A. 1987. Active tectonics of the Adriatic region. *Geophys. J. R.*
411 *Astron. Soc.*, 91, 937–983.
- 412 2. Balogh, K., Colantoni, P., Guerrera, F., Majer, V., Ravasz-Baranyai, L., Renzulli, A., Veneri, F. and
413 Alberini, C. 1994. The Medium-Grained Gabbro of the Jabuka Islet. *Scoglio del Pomo, Adriatic Sea.*
- 414 3. Bennett, R., Hreinsdottir, S., Buble, G., Basic, T., Bacic, Z., Marjanovic, M., Casale, G., Gendaszek, A.
415 and Cowan, D. 2008. Eocene to present subduction of southern Adria mantle lithosphere beneath
416 the Dinarides. *Geology* 36 (1), 3–6, <http://dx.doi.org/10.1130/G24136A.1>
- 417 4. Bernoulli, D. 2007. The pre-Alpine geodynamic evolution of the Southern Alps: A short summary.
418 *Bulletin für angewandte Geologie*, 12(2), 3–10.
- 419 5. Buser, S. 1987. Development of the Dinaric and Julian carbonate platforms and of the intermediate
420 Slovenian basin (NW Yugoslavia). *Memorie della Societa Geologica Italiana*, 40, 313–320.
- 421 6. Butler, R. W. H., Mazzoli, S., Corrado, S., De Donatis, M., Di Bucci, D., Gambini, R., Naso, G., Nicolai,
422 C., Scrocca, D., Shiner, P. and Zucconi, V. 2004. Applying thick-skinned tectonic models to the
423 Apennine thrust belt of Italy—Limitations and implications. In: K. R. McClay (eds) *Thrust tectonics*
424 *and hydrocarbon systems: AAPG Memoir 82*, p. 647–667.
- 425 7. Calcagnile, G. and Panza, G. F. 1981. The main characteristics of the lithosphere-asthenosphere
426 system in Italy and surrounding regions. *Pure and Applied Geophysics* 119, 865-879.
- 427 8. Caratori Tontini, F., Stefanelli, P., Giori, I., Faggioni, O. and Carmisciano, c. 2004. The revised
428 aeromagnetic anomaly map of Italy. *Annals of Geophysics* V. 47, N. 5.
- 429 9. Cassinis, G., Cortesogno, L., Gaggero, L., Perotti, C. R. and Buzzi, L. 2008. Permian to Triassic
430 geodynamic and magmatic evolution of the Brescian Alps (eastern Lombardy, Italy). In G. Cassinis
431 (Ed.), Vol. 127(3). *Stratigraphy and palaeogeography of late- and post-hercynian basins in the*
432 *Southern Alps, Tuscany and Sardinia (Italy)* (pp. 501–518). Rome: *Italian Journal of Geosciences*
433 *(Bollettino della Societa Geologica Italiana)*.
- 434 10. Cassinis, G., Perotti, C. R. and Ronchi, A. 2012. Permian continental basins in the Southern Alps
435 (Italy) and peri-mediterranean correlations. *International Journal of Earth Sciences (Geologische*
436 *Rundschau)*, 101, 129–157. <http://dx.doi.org/10.1007/s00531-011-0642-6>.
- 437 11. Cazzola, C. and Soudet, H. J. 1993. Facies and Reservoir Characterization of Cretaceous-Eocene
438 Turbidites in the Northern Adriatic. In: Spencer A.M. (eds) *Generation, Accumulation and*
439 *Production of Europe’s Hydrocarbons III. Special Publication of the European Association of*
440 *Petroleum Geoscientists*, vol 3. Springer, Berlin, Heidelberg. [https://doi.org/10.1007/978-3-642-](https://doi.org/10.1007/978-3-642-77859-9_16)
441 [77859-9_16](https://doi.org/10.1007/978-3-642-77859-9_16)
- 442 12. Chiappini, M., Meloni, A., Boschi, E., Faggioni, O., Beverini, N., Carmisciano, C., Marson, I., Magrini,
443 C. and Vongher, G. 2000. Onshore–Offshore Integrated Shaded Relief Magnetic Anomaly Map at

- 444 Sea Level of Italy and Surrounding Areas – Total Intensity. Data Reduction to Geomagnetic Epoch
445 1979.
- 446 13. CNR – PFG. 1991. Structural model of Italy and gravity map. Quaderni della Ricerca Scientifica, n.
447 114, vol. 3.
- 448 14. D’Agostino, N., Avallone, A., Cheloni, D., D’Anastasio, E., Mantenuto, S. and Selvaggi, G. 2008.
449 Active tectonics of the Adriatic region from GPS and earthquake slip vectors. *Journal of Geophysical*
450 *Research* 113, doi:10.1029/2008JB005860.
- 451 15. Di Bucci, D., Ravaglia, A., Seno, S., Toscani, G., Fracassi, U. and Velnsise G. 2006. Seismotectonics of
452 the southern Apennines and Adriatic foreland: Insights on active regional E-W shear zones from
453 analogue modeling. *Tectonics* 25, TC4015, doi:10.1029/2005TC001898.
- 454 16. Doglioni, C., Mongelli, F. and Pieri, P. 1994. The Puglia uplift (SE Italy): an anomaly in the foreland of
455 the Apenninic subduction due to buckling of a thick continental lithosphere. *Tectonics* 13, N. 5,
456 doi:10.1029/94TC01501.
- 457 17. Eyuboglu, Y., Dudas, F. O., Chatterjee, N., Liu, Z. and Yilmaz-Değeri, S. 2018. Discovery of Latest
458 Cretaceous OIB-type alkaline gabbros in the Eastern Pontides Orogenic Belt, NE Turkey: Evidence
459 for tectonic emplacement of seamounts. *Lithos*, 310-311, 182-200.
- 460 18. Faccenna, C., Becker, T. W., Auer, L., Billi, A., Boschi, L., et al. 2014. Mantle dynamics in the
461 Mediterranean. *Review of Geophysics*, 52, 283-332.
- 462 19. Federici, I., Cavazza, W., Okay, A. I., Beyssac, O., Zattin, M., Corrado, S. and Dellisanti, F. 2010.
463 Thermal Evolution of the Permo–Triassic Karakaya Subduction-accretion Complex between the Biga
464 Peninsula and the Tokat Massif (Anatolia). *Turkish Journal of Earth Sciences* 19, 409-429.
465 doi:10.3906/yer-0910-39
- 466 20. Gaetani, M. 2010. From Permian to cretaceous: Adria as pivotal between extensions and rotations
467 of Tethys and Atlantic Oceans. In M. Beltrando, A. Peccerillo, M. Mattei, S. Conticelli, & C. Doglioni
468 (Eds.), *The geology of Italy: Tectonics and life along plate margins*. *Journal of the Virtual Explorer*,
469 36. <http://dx.doi.org/10.3809/jvirtex.2010.00235>. paper no. 6, Electronic Edition.
- 470 21. Giori, I., Caratori Tontini, F., Cocchi, L., Carmisciano, C., Bologna, C., Camorali, C., Samarzija, J. And
471 Taylor, P. 2007. The Adriatic Magnetic Anomaly. EGM 2007 International Workshop, Capri – Italy
472 16-18 april 2007.
- 473 22. Handy, M. R., Giese, J., Schmid, S. M., Pleuger, J., Spakman, W., Nuzi, K. and Ustaszewski, K. 2019.
474 Coupled crust-mantle response to slab tearing, bending and rollback along the Dinaride-Hellenide
475 orogen. *Tectonics*, doi:10.1029/2019TC005524.
- 476 23. Herak, M. 1986. A new concept of geotectonics of the Dinarides. *Acta Geol.* 16, 1–42.
- 477 24. Juracic, M., Novosel, A., Tibljas, D. and Balen, D. 2004. Jabuka shoal, a new location with igneous
478 rocks in the Adriatic Sea. *Geol. Croat.* 57 (1), 81–85.

- 479 25. Korbar, T. 2009. Orogenic evolution of the External Dinarides in the NE Adriatic region: a model
480 constrained by tectonostratigraphy of Upper Cretaceous to Paleogene carbonates. *Earth Sci. Rev.*
481 96, 296–312.
- 482 26. Mancinelli, P., Pauselli, C., Minelli, G. and Federico, C. 2015. Magnetic and gravimetric modeling of
483 the Central Adriatic region. *Journal of Geodynamics* 89, 60-70.
- 484 27. Mancinelli, P., Pauselli, C., Minelli, G., Barchi, M. R. and Simpson, G. 2018. Potential evidence for
485 slab detachment from the flexural backstripping of a foredeep: Insight on the evolution of the
486 Pescara basin (Italy). *Terra Nova* 2018, 1-11, DOI: 10.1111/ter.12329.
- 487 28. Mancinelli, P., Porreca, M., Pauselli, C., Minelli, G., Barchi, M. R. and Speranza, F. 2019. Gravity and
488 Magnetic Modeling of Central Italy: Insights Into the Depth Extent of the Seismogenic Layer.
489 *Geochemistry, Geophysics, Geosystems*, 20, <https://doi.org/10.1029/2018GC008002>.
- 490 29. Menant, A., Angiboust, S. and Gerya, T. 2019. Stress-driven fluid flow controls long-term
491 megathrust strength and deep accretionary dynamics. *Scientific Reports* 9:9714
492 <https://doi.org/10.1038/s41598-019-46191-y>
- 493 30. Menant, A., Angiboust, S., Gerya, T., Lacassin, R., Simoes, M. and Grandin, R. 2020. Transient
494 stripping of subducting slabs controls periodic forearc uplift. *Nature Communications*, 11:1823
495 <https://doi.org/10.1038/s41467-020-15580-7>
- 496 31. Milano, M. and Fedi, M. 2016. Multiscale study of the Adriatic Magnetic Anomaly. *NGTGS 2016*,
497 sessione 3.1.
- 498 32. Milano, M., Fedi, M. and Fairhead, J. D. 2019. Joint analysis of the magnetic field and total gradient
499 intensity in Central Europe. *Solid Earth* 10, 697-712.
- 500 33. Minelli, L., Speranza, F., Nicolosi, I., D'Ajello Caracciolo, F., Carluccio, R., Chiappini, S., et al. 2018.
501 Aeromagnetic investigation of the Central Apennine Seismogenic Zone (Italy): From basins to faults.
502 *Tectonics*, 37, 1435–1453. <https://doi.org/10.1002/2017TC004953>
- 503 34. Moix, P., Beccaletto, L., Kozur, H., Hochard, C., Rosselet, F. and Stampfli G. M. 2008. A new
504 classification of the Turkish terranes and sutures and its implication for the paleotectonic history of
505 the region. *Tectonophysics* 451, 7–39
- 506 35. Moix, P., Vachard, D., Allibon, J., Martini, R., Wernli, R., Kozur, H. W. and Stampfli, G. M. 2013.
507 Palaeotethyan, Neotethyan and Huğlu-Pindos Series in the Lycian Nappes (SW Turkey):
508 Geodynamical Implications. In: Tanner, L.H., Spielmann, J.A. and Lucas, S.G., eds., 2013, *The Triassic*
509 *System*. New Mexico Museum of Natural History and Science, Bulletin 61.
- 510 36. Moretti, I. and Royden, L. 1988. Deflection, gravity-anomalies and tectonics of doubly subducted
511 continental lithosphere – Adriatic and Ionian seas. *Tectonics* 7, 875–893.

- 512 37. Nakanishi, A., Kurashimo, E., Tatsumi, Y., et al. 2009. Crustal evolution of the southwestern Kuril
513 Arc, Hokkaido Japan, deduced from seismic velocity and geochemical structure. *Tectonophysics*
514 472, 105–123.
- 515 38. Nicolich, R. 2001. Deep seismic transects. In: Vai, G.B., Martini, I.P. (Eds.), *Anatomy of an Orogen:*
516 *The Apennines and Adjacent Mediterranean Basins.* Kluwer Academic Publishers, Dordrecht, The
517 Netherlands, pp. 47–52.
- 518 39. Oldow, J. S., Ferranti, L., Lewis, D. S., Campbell, J. K., D’Argenio, B., Catalano, R., Pappone, G.,
519 Carmignani, L. and Aiken, C. L. V. 2002. Active fragmentation of Adria, the north African
520 promontory, central Mediterranean orogen. *Geology*, 30 (9), 779.
- 521 40. Palinkaš, L. A., Borojević Šošćarić, S., Strmić Palinkaš, S., Crnjaković, M., Neubauer, F., Molnár, F. and
522 Bermanec, V. 2010. Volcanoes in the Adriatic Sea: Permo-Triassic magmatism on the Adriatic–
523 Dinaridic carbonate platform. *Acta Mineralogica-Petrographica, Field Guide Series, Vol. 8, PP. 1–15*
- 524 41. Pamić, J. and Balen, D. 2005. Interaction between Permo-Triassic rifting, magmatism and initiation
525 of the Adriatic-Dinaric Carbonate platform (ADCP). *Acta Geol. Hung.* 48 (2), 181–204.
- 526 42. Scarascia, S., Cassinis, R. and Federici, F. 1998. Gravity modelling of deep structures in the
527 Northern-Central Apennines. *Memorie della Società Geologica Italiana* 52, 231-246.
- 528 43. Schuster, R. and Stüwe, K. 2008. Permian metamorphic event in the Alps. *Geology* 36; no. 8; p. 603–
529 606; doi: 10.1130/G24703A.1.
- 530 44. Scisciani, V. and Eserstine, P. 2017. The Triassic Evaporites in the Evolution of the Adriatic Basin. In:
531 *Permo-Triassic salt provinces of Europe, North Africa and the Atlantic Margins.*
532 <http://dx.doi.org/10.1016/B978-0-12-809417-4.00024-0>, Elsevier.
- 533 45. Scrocca, D., Doglioni, C., Innocenti, F., Manetti, P., Mazzotti, A., Bertelli, L., Burbi, L. and D’Offizi, S.
534 (Eds.) 2003. *CROP Atlas: seismic reflection profiles of the Italian crust.* *Memorie Descrittive della*
535 *Carta Geologica d’Italia*, 62: pp. 194.
- 536 46. Stampfli, G.M. and Borel, G.D., 2004. The TRANSMED Transects in Space and Time: constraints on
537 the Paleotectonic Evolution of the Mediterranean Domain. In: Cavazza W., Roure F., Spakman W.,
538 Stampfli G.M., Ziegler P.A. (eds) *The TRANSMED Atlas. The Mediterranean Region from Crust to*
539 *Mantle.* Springer, Berlin, Heidelberg. https://doi.org/10.1007/978-3-642-18919-7_3
- 540 47. Stampfli, G. M. and Kozur, H. W. 2006. Europe from the Variscan to the Alpine cycles. In: D.G. Gee
541 and R. Stephenson (Editors), *European lithosphere dynamics. Memoir of the Geological Society*
542 (London) 32, 57-82.
- 543 48. Stampfli, G. M. and Hochard, C. 2009. Plate tectonics of the Alpine realm. In: Murphy, J.B., Hynes,
544 A.J. and Keppie, J.D., eds, *Ancient orogens and modern analogues*, *Geol. Soc. London Spec. P.*,
545 327,89-111.

- 546 49. Stampfli G. M., Hochard, C., Vérard, C., Wilhem, C. and von Raumer, J. 2013. The formation of
547 Pangea. *Tectonophysics* 593, 1-19.
- 548 50. Stein, S., and Sella, G. 2005. Pleistocene change from convergence to extension in the Apennines as
549 a consequence of Adria microplate motion, in *The Adria Microplate: GPS Geodesy, Tectonics and*
550 *Hazards*, Nato Sci. Ser., edited by N. Pinter et al., pp. 21–34, Springer, Berlin, Germany.
- 551 51. Sumanovac, F., 2010. Lithosphere structure at the contact of the Adriatic microplate and the
552 Pannonian segment based on the gravity modeling. *Tectonophysics* 485, 94–106.
- 553 52. Sun, W., Zhao, L., Malusà, M. G., Guillot, S. and Fu, Li-Y. 2019. 3-D Pn tomography reveals
554 continental subduction at the boundaries of the Adriatic microplate in the absence of a precursor
555 oceanic slab. *Earth and Planetary Science Letters* 510, 131-141.
- 556 53. Tari, V., 2002. Evolution of the northern and western Dinarides: a tectonostratigraphic approach.
557 EGU Stephan Mueller Special Publication Series, vol. 1., pp. 223–236.
- 558 54. Tassis, G.A., Grigoriadis, V.N., Tziavos, I.N., Tsokas, G.N., Papazachos, C.B. and Vasiljevic, I., 2013. A
559 new Bouguer gravity anomaly field for the Adriatic Sea and its application for the study of the
560 crustal and upper mantle structure. *J. Geodyn.* 66, 38–52.
- 561 55. Thybo, H. and Artemieva, I. M. 2013. Moho and magmatic underplating in continental lithosphere.
562 *Tectonophysics* 609, 605-619.
- 563 56. van Unen, M., Matenco, L., Nader, F. H., Darnault, R., Mandic, O. and Demir, V. 2019. Kinematics of
564 Foreland-Vergent Crustal Accretion: Inferences From the Dinarides Evolution. *Tectonics* 38, 49–76.
565 <https://doi.org/10.1029/2018TC005066>
- 566 57. Vavassis, I., De Bono, A., Stampfli, G. M., Giorgis, D., Valloton, A. and Amelin, Y. 2000. U-Pb and Ar-
567 Ar geochronological data from the Pelagonian basement in Evia (Greece): geodynamic implications
568 for the evolution of Paleotethys. *Schweizerische Mineralogische und Petrographische Mitteilungen*
569 80: 21-43.
- 570 58. Velić, I., Vlahović, I. and Matičec, D. 2002. Depositional sequences and palaeogeography of the
571 Adriatic carbonate platform. *Memorie della Società Geologica Italiana*, 57, 141–151.
- 572 59. Watts, A. B. 2001. *Isostasy and flexure of the lithosphere*. Cambridge University Press, Cambridge.
- 573 60. Zandt, G., Myers, S. C. and Wallace, T. C. 1995. Crust and mantle structure across the Basin and
574 Range – Colorado Plateau boundary at 37°N latitude and implications for Cenozoic extensional
575 mechanism. *Journal of Geophysical Research* 100, NO. B6, 10529 doi: 10.1029/94JB03063

576

577 **References_Methods**

- 578 1. Atlas of Geothermal resources in Europe. 2002. Plate 1 of the Heat-Flow density over Europe.
579 European Community Publ. Nr. EUR 17811.

- 580 2. Bronner, A., Sauter, D., Manatschal, G., Péron-Pinvidic, G. and Munsch, M. 2011. Magmatic
581 breakup as an explanation for magnetic anomalies at magma-poor rifted margins. *Nature*
582 *Geoscience* 4, 549-553.
- 583 3. Della Vedova, B., Bellani, S., Pellis, G. and Squarci, P. 2001. Deep temperatures and surface heat
584 flow distribution. In: Vai, G.B., Martini, I.P. (Eds.), *Anatomy of an Orogen: The Apennines and*
585 *Adjacent Mediterranean Basins*. Kluwer Academic Publishers, Dordrecht, The Netherlands, pp. 65–
586 76.
- 587 4. Fourier, J. 1822. *Théorie analytique de la chaleur*. Paris: Firmin Didot Père et Fils.
- 588 5. Frost, B. R., and Shive, P. N. 1986. Magnetic mineralogy of the lower continental crust. *Journal of*
589 *Geophysical Research*, 91(B6), 6513–6521. <https://doi.org/10.1029/JB091iB06p06513>
- 590 6. Kurevija, T., Vulin, D. and Macenic, M. 2014. Impact of geothermal gradient on ground source heat
591 pump system modeling. *Rudarsko-geološko-naftni zbornik vol 28*, 39-45.
- 592 7. Pauselli, C., Barchi, M. R., Federico, C., Magnani, M. B., and Minelli, G. 2006. The crustal structure of
593 the Northern Apennines (Central Italy): An insight by the CROP03 seismic line. *American Journal of*
594 *Science*, 306(6), 428–450. <https://doi.org/10.2475/06.2006.02>
- 595 8. Pauselli, C. and Ranalli, G. 2017. Effects of lateral variations of crustal rheology on the occurrence
596 post-orogenic normal faults: The Alto Tiberina Fault (Northern Apennines, Central Italy).
597 *Tectonophysics*, 721, 45–55.
- 598 9. Pauselli, C., Gola, G., Mancinelli, P., Trumpy, E., Saccone, M., Manzella, A. and Ranalli G. 2019. A
599 new surface heat flow map of the Northern Apennines between latitudes 42.5 and 44.5 N.
600 *Geothermics* 81, 39-52.
- 601 10. Petford, N., Cruden, A.R. and McCaffrey, K.J.W., et al. 2000. Granite magma formation, transport
602 and emplacement in the Earth's crust. *Nature* 408, 669–673.
- 603 11. Pullaiah, G., Irving, E., Buchan, K. L. and Dunlop, D. J. 1975. Magnetization changes caused by burial
604 and uplift. *Earth and Planetary Science Letters*, 28, 133–143.
- 605 12. Punturo, R., Mamtani, M. A., Fazio, E., Occhipinti, R., Renjith, A. R. and Cirrincione, R. 2017. Seismic
606 and magnetic susceptibility anisotropy of middle-lower continental crust: Insights for their
607 potential relationship from a study of intrusive rocks from the Serre Massif (Calabria, southern
608 Italy). *Tectonophysics*, 712(713), 542–556. <https://doi.org/10.1016/j.tecto.2017.06.020>
- 609 13. Rochette, P. 1994. Comments on “Anisotropic magnetic susceptibility in the continental lower crust
610 and its implication for the shape of magnetic anomalies” by G. Florio et al. *Geophysical Research*
611 *Letters*, 21, 2773–2774.
- 612 14. Schlinger, C. M. 1985. Magnetization of lower crust and interpretation of regional magnetic
613 anomalies: Example from Lofoten and Vesterrålen, Norway. *Journal of Geophysical Research*,
614 90(B13), 11,484–11,504.


- 615 15. Shive, P. N., Blakely, R. J., Frost, B. R., and Fountain, D. M. 1992. Magnetic properties of the lower
616 continental crust. In D. M. Fountain, R. Arculus, & R. W. Kay (Eds.), *Continental lower crust* (pp.
617 145–177). New York: Elsevier Sci.
- 618 16. Turcotte, D. L. and Schubert, G. 2002. *Geodynamics*. Cambridge University Press, Cambridge.
- 619 17. Van der Voo, R. 1990. Phanerozoic paleomagnetic poles from Europe and North America and
620 comparisons with continental reconstructions. *Reviews of Geophysics* 28, 167-206.
- 621 18. Wasilewski, P. J., Thomas, H. H., and Mayhew, M. A. 1979. The Moho as a magnetic boundary.
622 *Geophysical Research Letters*, 6(7), 544–541
- 623 19. Wasilewski, P. J., and Mayhew, M. A. 1992. The Moho as a magnetic boundary revisited.
624 *Geophysical Research Letters*, 19(22), 2259–2262.

625


626

Supplementary material for the manuscript

627 **Back-arc underplating provides crustal accretion affecting topographic and**
628 **sedimentary domains.**

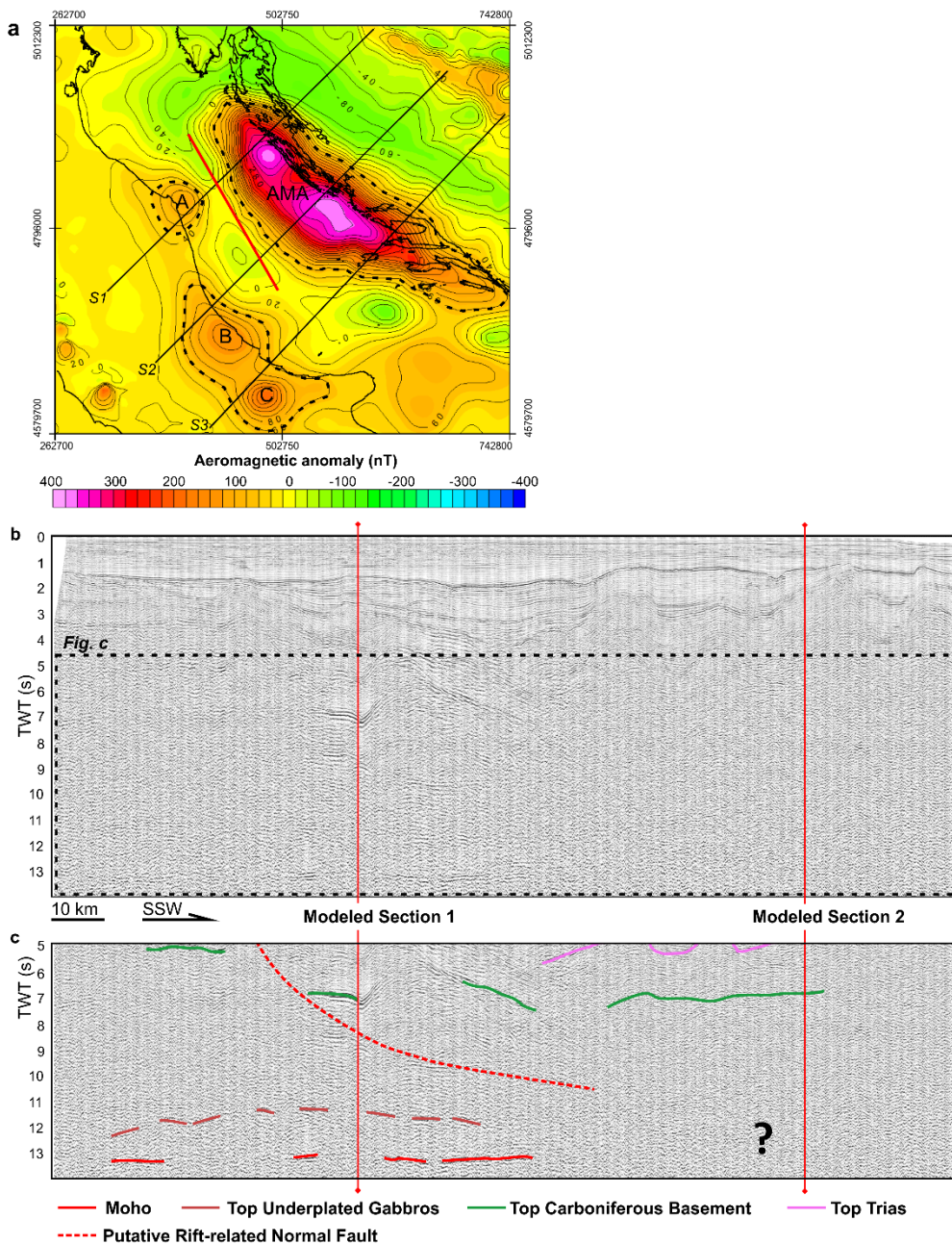
629 Paolo Mancinelli, Vittorio Scisciani, Cristina Pauselli, Gérard M. Stampfli, , Ivana Vasiljevic

630

631 This supplementary material consists of  2 figures and supplementary text.

632

Figure S1



633

634 **Figure S1. Location and interpretation of the seismic reflection profile CROP M17C.** a, Location of the
635 CROP M17C profile (red line) across the study area. b, clean image of the CROP M17C profile between 0

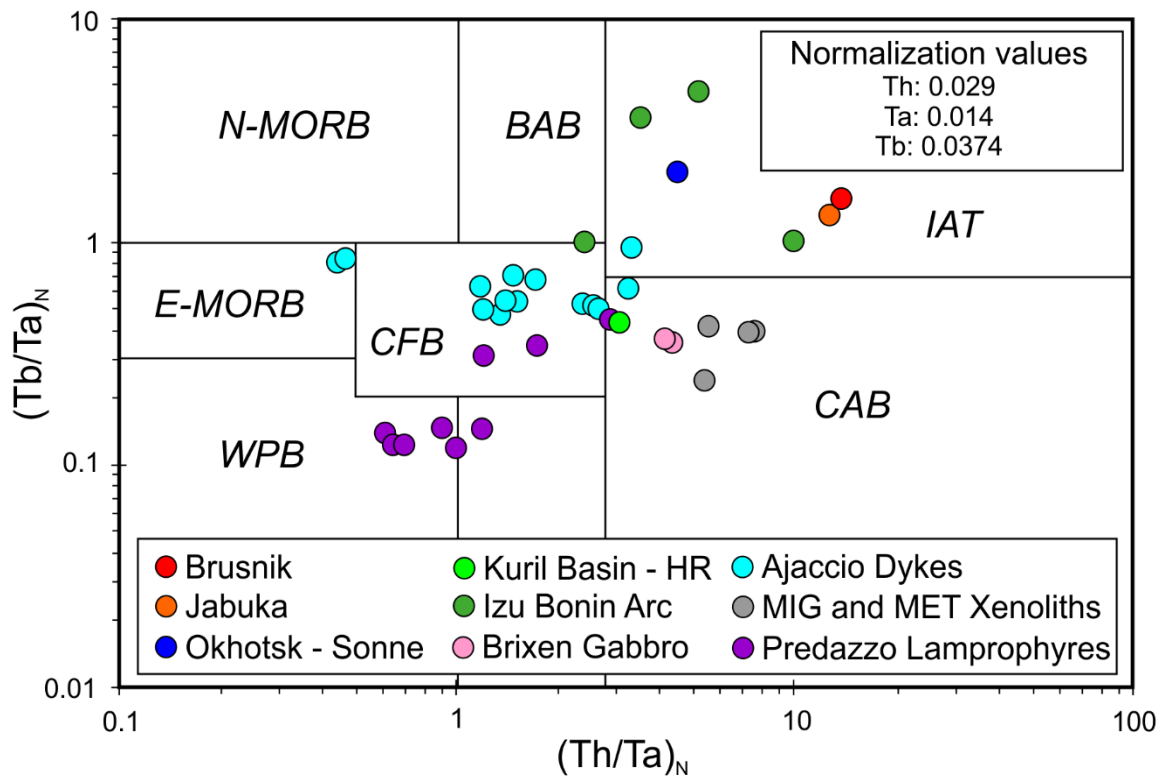
636 and 14 sec TWT. Red vertical lines locate the intersection with modeled sections 1 and 2. **c**, Interpretative
637 sketch of the main horizons between 5 and 14 sec TWT.

638

639 **Figure S1** shows the interpretation of the deep main horizons in the study area. This line represents the
640 best deep (> 6 s TWT) seismic data across the entire Central Adriatic Sea because in its northernmost
641 portion some deep reflectors are traceable. In particular, we locate the ~13 sec TWT horizon that we
642 interpret as representative of the Moho discontinuity, we also locate some discontinuous reflections above
643 the Moho between 11 and 12 sec TWT (brown horizons) and some other shallow reflections interpreted as
644 the top of the carboniferous basement (green horizons) and the top of the Triassic sequence (pink
645 horizons) in the southern region.

646

Figure S2



648

649 **Figure S2. $(Th/Ta)_N$ vs $(Tb/Ta)_N$ ratios (Thièblemont et al., 1994) for the gabbros outcropping in Jabuka**
 650 **and Brusnik islands compared with surrounding known Permian-Triassic volcanics and intrusives and**
 651 **with the Okhotsk-Kuril arc and the Izu Bonin arc volcanics.** N-MORB field – N-Type MORB; E-MORB
 652 field – E-Type MORB; BAB field – Oceanic back-arc basin basalt; WPB field – Within-plate basalt
 653 (transitional and alkaline); CFB field – Continental tholeiite; IAT – Island-arc tholeiite; CAB – Subduction-
 654 related calc-alkaline lava. These data exclude a basaltic composition and a seamount origin for the
 655 gabbros outcropping in Jabuka and Brusnik (see Figure 1 for their locations). Brusnik and Jabuka
 656 compositional data are from Radić and Lugović (2004). Data from the Sonne volcanoes in the Okhotsk
 657 Sea and from the Hydrographer Ridge (HR) in the Kuril Basin correspond to samples 126-1-1, 126-1-2,
 658 DR7-1-1, DR7-1-2 and DR83-1-1 from Werner et al. (2020). Data from the Ajaccio dykes and Brixen
 659 gabbros are from Boscaini et al. (2020). Data from the Predazzo lamprophyre are from Casetta et al.
 660 (2019). Data from the Migmatite (MI) and Metapelite (ME) xenoliths are from the Euganean hills (Sassi
 661 et al., 2020). Data from the Izu Bonin arc are from Straub (2003). All data are normalized against CI
 662 Chondrites (Sun and McDonough, 1989).

663

664 **Figure S2** shows that when compared against data from an actual island-arc system in the Okhotsk Sea
 665 and Kuril Basin (Werner et al., 2020), the trace element composition of the Jabuka and Brusnik gabbros
 666 suggests that these are related to an internal back-arc area of the island-arc system. In fact, Jabuka and
 667 Brusnik samples shows a better fit with the Sonne samples (~300 km from the Kuril arc) rather than
 668 with the Hydrographer Ridge (HR) samples (~80 km from the Kuril arc). Moreover, the Jabuka and
 669 Brusnik samples are comparable also with the Izu Bonin back-arc volcanics (Straub, 2003). Finally, the
 670 trace element composition of the gabbros from jabuka and Brusnik do not compare with the

671 composition of the surrounding known Permian-Triassic volcanics and intrusives where such data are
672 available.

673

674 **References for the supplementary material**

- 675 1. Boscaini, A., Marzoli, A., Davies, J. F. H. L., Chiaradia, M., Bertrand, H., Zanetti, A., Visonà, D., De
676 Min, A. and Jourdan, F. 2020. Permian post-collisional basic magmatism from Corsica to the
677 Southeastern Alps. *Lithos*, 376-377, 105733, <https://doi.org/10.1016/j.lithos.2020.105733>.
- 678 2. Cassetta, F., Ickert, R. B., Mark, D. F., Bonadiman, C., Giacomoni, P. P., Ntaflos, T. and Coltorti,
679 M. 2019. The Alkaline Lamprophyres of the Dolomitic Area (Southern Alps, Italy): Markers of
680 the Late Triassic Change from Orogenic-like to Anorogenic Magmatism. *Journal of Petrology*, 1-
681 36, doi: 10.1093/petrology/egz031.
- 682 3. Radić, D. and Lugović, B. 2004. Petrographic and geochemical correlation between artifacts
683 from the mesolithic layers of Vela Spila and the magmatic rocks of Central Dalmatian Islands.
684 *Dalmacija* 210.7, UDK: 902.66:903.2. Available from:
685 https://hrcak.srce.hr/index.php?lang=en&show=clanak&id_clanak_jezik=26610
- 686 4. Sassi, F., Mazzoli, C., Merle, R., Brombin, V., Chiaradia, M., Dunkley, D. J. and Marzoli, A. 2020.
687 HT-LP crustal syntectonic anatexis as a source of the Permian magmatism in the Eastern
688 Southern Alps: evidence from xenoliths in the Euganean trachytes (NE Italy). *Journal of the*
689 *Geological Society*, DOI: <https://doi.org/10.1144/jgs2020-031>.
- 690 5. Straub, S. 2003. The evolution of the Izu Bonin - Mariana volcanic arcs (NW Pacific) in terms of
691 major element chemistry. *Geochem. Geophys. Geosyst.*, 4(2), 1018,
692 doi:10.1029/2002GC000357.
- 693 6. Sun, S. -s. and McDonough, W. F. 1989. Chemical and isotopic systematics of oceanic basalts:
694 implications for mantle composition and processes. Geological Society, London, Special
695 Publications 1989, v.42; p. 313-345. doi: 10.1144/GSL.SP.1989.042.01.19
- 696 7. Thièblemont, D., Chevremont, P., Castaing, C. and Feybessej, L. 1994. La discrimination
697 géotectonique des roches magmatiques basiques par les éléments traces: réévaluation d'après
698 une base de données et application à la chaîne panafricaine du Togo. *Geodinamica Acta*, Paris,
699 7, 3, pp. 139-157.
- 700 8. Werner, R., Baranov, B., Hoernle, K., van den Bogaard, P., Hauff, F. and Tararin, I. 2020.
701 Discovery of Ancient Volcanoes in the Okhotsk Sea(Russia): New Constraints on the Opening
702 History of the Kurile Back Arc Basin. *Geosciences*, 2020, 10, 442;
703 doi:10.3390/geosciences10110442